Article

Experimental Characterization of Separate Absorption–Multiplication GaAs Staircase Avalanche Photodiodes under Continuous Laser Light Reveals Periodic Oscillations at High Gains

Matija Colja [1,*] , **Marco Cautero** [2] , **Fulvia Arfelli** [3,4] , **Michele Bertolo** [1] , **Giorgio Biasiol** [5] , **Simone Dal Zilio** [5] , **Francesco Driussi** [6] , **Ralf Hendrik Menk** [1,3,7] , **Silvio Modesti** [3,4,5] , **Pierpaolo Palestri** [6] , **Alessandro Pilotto** [6] and **Giuseppe Cautero** [1,3]

1   Elettra-Sincrotrone Trieste S.C.p.A., Area Science Park Basovizza, 34149 Trieste, Italy; michele.bertolo@elettra.eu (M.B.); ralf.menk@elettra.eu (R.H.M.); giuseppe.cautero@elettra.eu (G.C.)

2   Department of Engineering and Architecture, University of Trieste, 34127 Trieste, Italy; marco.cautero@phd.units.it

3   Istituto Nazionale di Fisica Nucleare, INFN Sezione di Trieste, 34127 Trieste, Italy; fulvia.arfelli@ts.infn.it (F.A.); silvio.modesti@ts.infn.it (S.M.)

4   Department of Physics, University of Trieste, 34127 Trieste, Italy

5   IOM CNR, Laboratorio TASC, Area Science Park Basovizza, 34149 Trieste, Italy; biasiol@iom.cnr.it (G.B.); Dalzilio@iom.cnr.it (S.D.Z.)

6   Polytechnic Department of Engineering and Architecture, University of Udine, 33100 Udine, Italy; francesco.driussi@uniud.it (F.D.); pierpaolo.palestri@uniud.it (P.P.); pilotto.alessandro@spes.uniud.it (A.P.)

7   Department of Medical Imaging, University of Saskatchewan, Saskatoon, SK S7N 5A2, Canada

*   Correspondence: matija.colja@elettra.eu

Abstract: In this work, we experimentally analyze the periodic oscillations that take place in staircase APDs with separate absorption and multiplication regions when operating under continuous laser light. These oscillations increase in frequency when the APD gain increases. We have verified that they are not affected by the parameters (gain and bandwidth) of the transimpedance amplifier, and thus originate inside the APD. The phenomenon is analyzed systematically by considering devices with different thicknesses of the absorption region. Possible physical interpretations related to the flux of holes generated by impact ionization are provided.

Keywords: GaAs separate absorption–multiplication avalanche photodiode (GaAs SAM-APD); anomalous oscillations; transimpedance amplifier

1. Introduction

Avalanche photodiodes (APDs) are among the best-known and most widely employed solid-state devices for single-photon detection, representing the state of the art in terms of radiation sensitivity [1–3]. These devices convert photons to electron–hole pairs and then multiply one of the carriers (in most cases the electrons), resulting in an amplified photocurrent that allows for the detection of very weak optical signals, boosting the amplified output above the noise floor of the photoreceiver's circuit.

In recent years, research has focused on identifying alternatives to silicon (Si) for APD manufacturing that are able to offer better performance in terms of speed or quantum efficiency.

Devices based on III-V compounds possess unique properties, making them suitable for photonics, radio-frequency and high-power device technologies [4]. Among these materials, GaAs has proven to be a good candidate due to its higher effective atomic number, which results in a substantially shorter absorption length compared to Si, especially for medium-hard X-rays, thus allowing for the achievement of higher efficiencies for a

given device thickness. Furthermore, the higher electron mobility of GaAs reduces the response time, and its direct energy bandgap of 1.42 eV at 300 K makes operation at room temperature possible. Therefore, GaAs APDs may be the optimal candidate for replacing Si-based devices in the medium-hard X-ray energy range.

One of the main issues with GaAs-based APDs is that the impact ionization coefficients of electrons and holes do not differ significantly. As a result, the multiplication process has a higher associated noise, which can significantly degrade the signal-to-noise ratio [5]. Over the years, these devices have seen some significant evolutions to reduce the multiplicative noise via the separation of the "absorption and photon–electron conversion" region from the "multiplication" region (separate absorption–multiplication APDs, SAM-APDs), and the band-gap engineering in the multiplication region [6–8].

Also, the development of devices able to detect hard X-rays more efficiently is an important part within the synchrotron community. For this reason, in recent years at the Elettra Sincrotrone laboratories, in collaboration with CNR-IOM (Consiglio Nazionale delle Ricerche-Istituto Officina dei Materiali) and the University of Udine, research has been undertaken on GaAs SAM-APDs with a multiplication region based on a superlattice staircase structure, which promotes only electron impact ionization (II) at discrete locations, hence reducing below one the ratio between the effective ionization coefficients of holes (β) and electrons (α).

APD noise characteristics are typically quantified through the excess noise factor (ENF), which represents the noise increment compared to a device with a noiseless multiplication (shot noise only). One of the most commonly employed experimental techniques for measuring the ENF involves applying a reverse bias voltage to the APD and measuring the photocurrent noise power spectral density (PSD) by using a signal analyzer. While performing this type of analysis on our devices, we noticed that the signal analyzer exhibited sudden variations in the acquired spectrum and the resulting ENF was considerably higher, especially in devices with a thicker absorption region. This prompted us to conduct a more detailed analysis on the output signal of the APD, which revealed the presence of unexpected oscillations that not only affected the ENF measurements obtained with the signal analyzer, but also the extraction of the multiplication gain from measurements. Although similar oscillations have been observed in the past under different conditions [9], this phenomenon was not thoroughly understood or studied. We believe that a better understanding of this effect will allow for a more robust evaluation of the device performance.

We conducted a thorough investigation of this phenomenon using devices that feature absorption regions of varying thicknesses, but with identical multiplication regions, with continuous laser photon flux and an experimental setup developed ad hoc. Our study revealed that when the multiplication becomes relevant, the output current begins to oscillate despite the input signal (the photon flux) being continuous. Moreover, we found that the oscillation frequency is directly proportional to the output current, and it increases as the reverse bias voltage and/or the input photon flux increase. The frequency range also changes depending on the thickness of the absorption region, so that a decrease in thickness results in an increase in the oscillation frequency.

In Section 2, we will describe the fabricated devices and their main characteristics, and we will outline the experimental setup used for measuring the oscillations. In Section 3, we will present the experimental data. Finally, we will propose and discuss a qualitative model aimed at explaining this phenomenon.

2. Materials and Methods

2.1. Devices Structure and Mode of Operation

The general structure of the GaAs SAM-APDs considered in this work is schematically illustrated in Figure 1. Photons enter the device from the upper part of the mesa, through the input window, which includes an ohmic contact with a layer of p-doped GaAs; then, the GaAs epitaxial absorption layer converts photons into electron–hole pairs. The electron's multiplication process takes place in the following multiplication region. For the correct

operation, a reverse bias is applied between the p+ and n+ contacts and a p-doped δ layer, often referred as "charge layer", is used to separate the absorption and multiplication regions, which is essential for establishing a high electric field only in the latter, thus reducing the probability of multiplication in the absorption region.

The idea behind the design of these SAM-APDs is to create a region of pure absorption where multiplication does not occur, reducing the randomness of the multiplication process. For the same reason, a staircase structure is deployed in the multiplication region, which creates well-defined steps in the band diagram, promoting the electron impact ionization and thus reducing the multiplicative noise.

A detailed description of the fabrication process can be found in [10,11]. Mesa diodes with 200 μm diameter are fabricated with different thicknesses of the absorption region ($d_{abs} = 300$ nm, 4.5 μm and 15 μm) in order to observe the influence of this parameter on the oscillatory behavior.
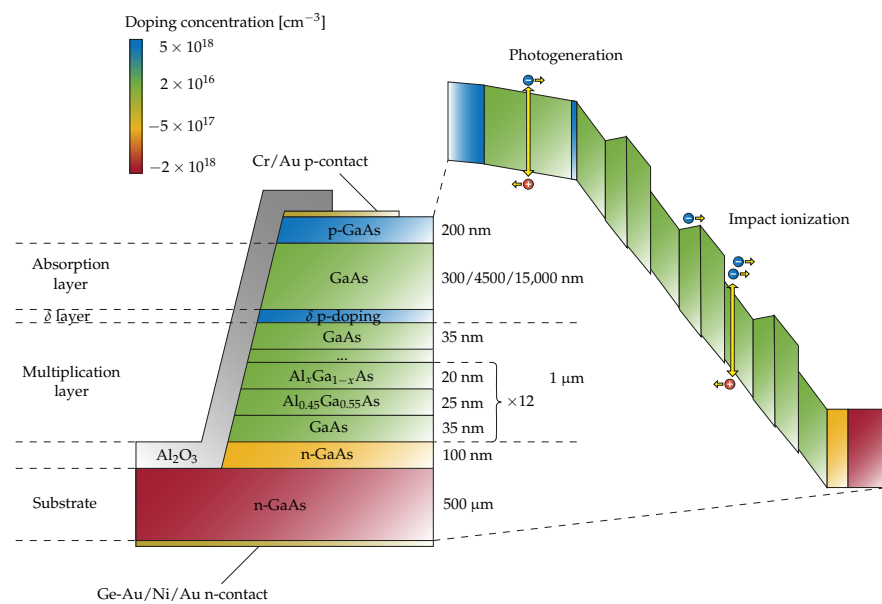

Figure 1. Sketch of the GaAs APD considered in this work (not to scale). The grown layered structure is depicted on the left side, where the layer color represents its doping concentration. The right plot sketches the band diagram under the reverse bias. In this figure, positive and negative doping concentrations are used for acceptors and donors, respectively.

2.2. Experimental Setup

2.2.1. Measurements under Dark Conditions

The devices were initially characterized by measuring the capacitance and current as a function of the reverse bias voltage. These measurements allow for the determination of the internal impedance (for small signals) as a function of the reverse bias, providing information about the electric field and potential distribution inside the APDs.

Capacitance measurements were performed using a high-precision LCR meter (Keysight Technology, HP4284A) at 1 MHz (more details in [10]), and we measured the current versus reverse bias characteristics (I-V curves) using a commercial transimpedance amplifier (TIA, AH501B Picoammeter [12]) to determine the internal resistance and breakdown voltage of the devices.

2.2.2. Measurements under Light Conditions

In order to characterize the fabricated devices and to highlight the oscillatory behavior observed under high photocurrent conditions, they were tested under light to assess their response to incoming photons, determining their gain and the noise induced by the multiplication process. A green (λ = 532 nm) tabletop laser was used, ensuring that

photogeneration took place entirely within the absorption region to avoid contamination with charges generated in the multiplication region. In fact, the absorption length in this energy range is approximately 160 nm, which is much shorter than the absorption regions of all our devices.

The gain M was calculated as the difference between the dark current I_{dark} and the measured photocurrent I_{tot} normalized by an exponential trend I_{ph}, obtained by interpolating the photocurrent from 10 V to 25 V (i.e., before multiplication takes place, as described in [10]), namely

$$M(V) = \frac{I_{tot}(V) - I_{dark}(V)}{a \cdot e^{bV}}, \tag{1}$$

where a and b are the parameters of the exponential trend extracted through the interpolation.

A custom TIA was developed with a lower gain (transresistance $R_{f1} = 5.6$ kΩ) and wider bandwidth (cutoff frequency $f_{c1} = 11$ MHz) for measuring the output current spectral density and estimating the noise introduced by the multiplication process. Its output voltage was fed into a signal analyzer (Agilent EXA N9010A) through a decoupling capacitor (see Figure 2a). The ENF was calculated by integrating the current spectral density S_i over a bandwidth B and then dividing it by the noise corresponding to noiseless multiplication (shot noise only), namely

$$ENF = \frac{\int_B S_i(f)\,df}{M^2 \cdot 2qI_{tot} \cdot B}. \tag{2}$$

In order to investigate the oscillations that are the topic of this article, the same setup was used, just replacing the signal analyzer with a 3 GHz analog bandwidth oscilloscope (Lecroy HDO9304), as shown in Figure 2b.
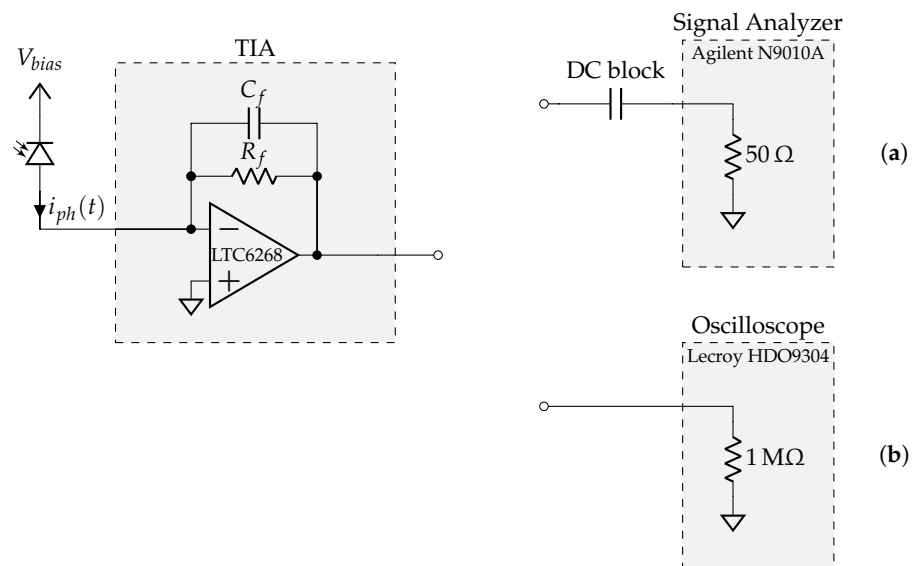

Figure 2. Front-end electronics used for PSD measurements (**a**) and oscillations measurements (**b**). While the input impedance of the signal analyzer is fixed to 50 Ω, for the oscilloscope, we selected high impedance to reduce the load of the TIA. We did not expect reflections associated with load mismatch, since the considered frequencies were lower than 100 MHz (wavelength 3 m) and the cable length was shorter than 30 cm.

We then analyzed two different trends: the output signal as a function of the bias voltage (fixed laser power $P_{laser} = 500$ μW) and as a function of the laser power (fixed bias $V = 36.5$ V). The oscillation phenomena appeared in the former in a voltage range between 35.5 V to 38 V, and in the latter within the entire laser power range (from 200 μW to 1 mW).

To be sure that this phenomenon was not an artifact of the measurement setup [13], we repeated the measurements by changing the amplifier's feedback network ($R_{f2} = 12$ kΩ

and $f_{c2} = 2.9$ MHz), obtaining exactly the same behavior, thus ruling out potential artifacts due to resonances in the circuit. Table 1 summarizes the main differences between the used TIAs.

Table 1. Parameters of the transimpedance amplifiers employed in this work.

TIA	R_f	C_f	f_c
	1.0 kΩ	15 nF	11 kHz
AH501B [1]	1.0 MΩ	15 pF	11 kHz
	1.0 GΩ	<0.5 pF	≈1 kHz
Custom-made TIA 1	5.6 kΩ	2.5 pF	11 MHz
Custom-made TIA 2	12 kΩ	4.5 pF	2.9 MHz

[1] Variable range.

3. Results

3.1. Capacitance

The C-V measurements are shown in Figure 3. The capacitance shows an initial drop (from 0 V to 5 V) given by the depletion of the multiplication region. The measured capacitance is comparable with the theoretical capacitance of a GaAs parallel-plate capacitor of the same dimensions of the detector (area $A = \pi \cdot (100\ \mu\text{m})^2$ and separation $d = 1\ \mu\text{m}$), which equals approximately 3.6 pF. Furthermore, even at higher bias values, there is no evident variation in the capacitance, showing that the absorption region does not get depleted. In other words, there is no evidence that punch-through takes place before breakdown. As a result, in the absorption region, the charges move exclusively by diffusion due to the negligible electric field. For biases higher than 36 V, the dark current starts to increase while the small-signal resistance rapidly decreases, prevailing on the capacitive impedance at 1 MHz, thus preventing accurate capacitance measurements.
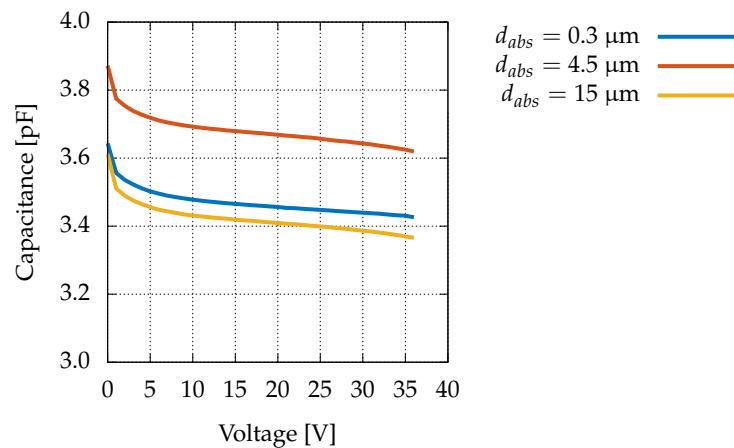

Figure 3. C-V measurement at 1 MHz of devices with different absorption region thicknesses. The small difference between the devices is due to to small geometrical differences in the areas, caused by the anisotropic nature of the etching process. We selected representative curves, but devices with the same nominal d_{abs} can show differences in capacitance up to 0.1 pF.

3.2. Gain

Measurements were initially carried out on devices with d_{abs} = 4.5 μm with P_{laser} = 500 μW. We first verified that the DC currents, obtained with different TIAs, were the same (see Figure 4a). In the figure, we see that the photogenerated current is very low, below approximately 4V. This voltage is required to compensate all the built-in potentials at the different (hetero)junctions. Then, the current increases exponentially with the bias. In fact, as shown in the CV curves of Figure 3, the devices do not reach punch-through in the measured range. This means that there is a barrier between the

absorption layer and the separation layer that would tend to prevent the flow of electrons. However, in our devices, this barrier is quite thin and low, so that a significant fraction of the photogenerated electrons can overcome it and enter the multiplication region. Carrier emission exponentially depends on the barrier height, which almost linearly depends on the applied bias, resulting in a photogenerated current that goes exponentially with the bias (see the exponential fitting provided by the dashed line). Since the output noise is proportional to the amplifier's bandwidth, the measurements with the wide-band TIAs refer to a limited bias range: for lower biases, the output signal is dominated by noise, whereas the TIA saturation voltage limits the maximum measurable current (and therefore the maximum bias). Since, as will be shown, the oscillations appear at approximately 36 V, we decided to limit our study to this voltage range (from 35.5 V to 38 V).

By using the DC photocurrent, we calculated the device gain by subtracting the dark current and normalizing by the exponential trend interpolated from 10 V to 25 V (see the black dashed line in Figure 4a). The resulting gain is shown in Figure 4b. The gain starts to increase at approximately 25 V, reaching its maximum ($M_{max} = 12$) at 37.375 V. For higher biases, the dark current significantly increases, reducing the resulting gain.
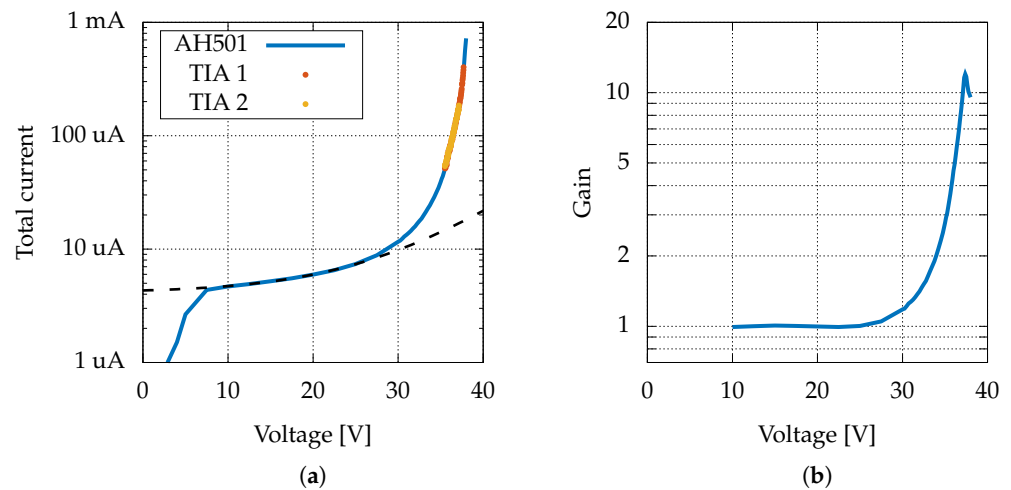

Figure 4. (**a**) Output DC current with $P_{laser} = 500$ μW as a function of the bias voltage. Comparison between measurements performed with AH501 and custom-made TIAs (see Table 1). (**b**) Gain as a function of the reverse bias for a device with $d_{abs} = 4.5$ μm.

3.3. Excess Noise Factor

The ENF values obtained using Equation (2) and the setup in Figure 2a are reported in Figure 5 for the devices with different absorption regions. It can be seen that for devices with $d_{abs} = 15$ μm, no ENF values are reported for M greater than 7, while for the remaining two thicknesses, ENF is reported up to $M = 20$. Above these values, an accurate ENF estimation is complicated, since fluctuations of the output current spectral density were observed, caused by the previously mentioned oscillations. The figure also reports the results of the local model. The value $k = \beta/\alpha$ is adjusted to match the results. Although the local model is not adequate to describe complex super-lattices as those present in our devices, the value of k of the local model is a good indication of the capabilities of the staircase structure to reduce the strength of hole impact ionization compared to electron one.
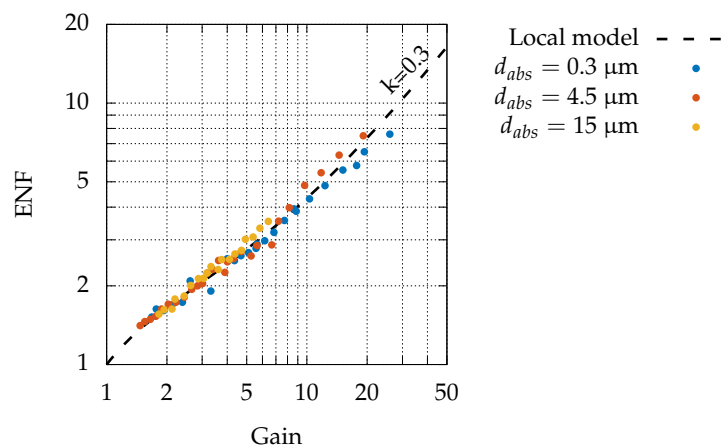
Figure 5. Extracted ENF for the three device types. The dashed line plots the trend of the local model [14] with $k = \beta/\alpha = 0.3$, the value that best matches the experimental ENF.

3.4. Oscillations at Fixed Laser Power

Employing a wide-band TIA allows one to investigate AC signals up to the frequency limited by its bandwidth. When observing the current waveforms at constant bias in the presence of multiplication, we noticed that suddenly, and in a reproducible way, in the transition from 35.9 V to 36.0 V, oscillations appear with a fairly precise dominant frequency close to 28 MHz, as shown in Figure 6 (time domain) and Figure 7 (frequency domain). The oscillation amplitude is comparable with the DC value, also considering the fact that the oscillation frequency is higher than the cutoff frequency of the TIA ($f_c = 11$ MHz), and therefore, its amplification is lower than the static gain.

As the reverse bias was increased, the oscillations were still present and their frequencies increased as well, and that trend continued up to 37 V. Figure 8 reports the spectrogram (i.e., the different spectra at each bias plotted one next to the other) from 35.5 V to 38 V in 25 mV steps, while Figure 9 illustrates the normalized oscillation amplitude of the main harmonic with increasing bias from 36.100 V to 36.550 V. The oscillation peak frequency increases with the bias, ranging from 30 MHz to 75 MHz. Figure 10 shows the amplitude of the current oscillation, which slightly decreases with frequency, suggesting a sort of internal cutoff mechanism. Overall, the changes in terms of amplitude are small, and so most of the information about the oscillation phenomena is embedded in its frequency. For this reason, in the following, we will focus our attention on the oscillation frequency.

Figure 11 plots the oscillation frequency (defined as the frequency of the maximum amplitude peak from 30 MHz to 100 MHz) as a function of the output DC current (Figure 11a) and of the current corresponding to the holes generated by impact ionization (Figure 11b). The hole current is computed as

$$I_h = (M - 1) \cdot I_{ph}, \tag{3}$$

where M is the gain and $I_{ph} = a \cdot e^{bV}$ is the interpolated exponential trend introduced in Equation (1).

For frequencies lower than 30 MHz, the identification of the oscillation peak was challenging due to a spurious signal of approximately 25 MHz coupling with the measurement setup (visible in Figure 8 as a light horizontal line), whereas frequencies above 100 MHz were significantly greater than the cutoff frequency of the TIA amplifier, and therefore, the TIA gain was considerably lower, attenuating the signal below the noise floor. The trends in Figure 11 are essentially linear, both considering as the x-axis the total current in the APD and the hole current generated by impact ionization in the multiplication region and then injected into the absorption region. This means that a larger amount of photogenerated current (and associated holes generated by impact ionization) results in an increase in the oscillation frequency. Possible explanations will be discussed later. In

Figure 11, we furthermore see that with both TIAs, the oscillation frequency values are similar, confirming that the oscillations were not influenced by the front-end electronics used to perform the measurements.
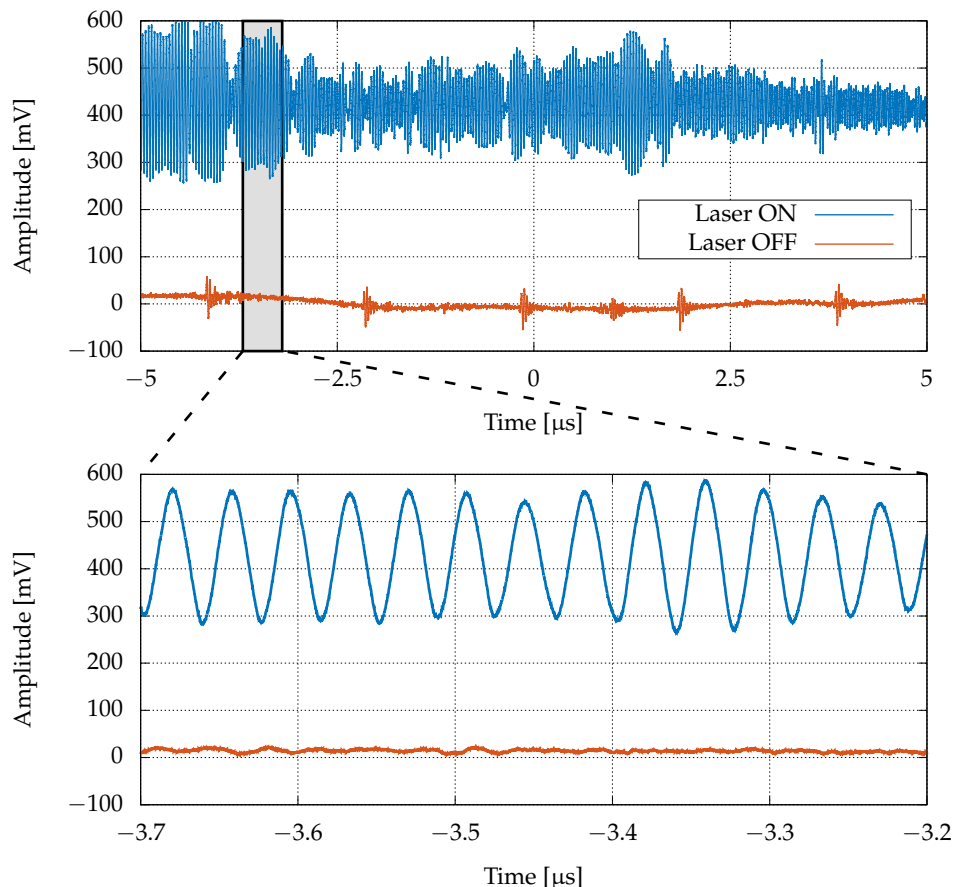

Figure 6. Oscillations in a device with $d_{abs} = 4.5$ μm at $V = 36.0$ V with $P_{laser} = 500$ μW measured with TIA 1. The traces were acquired in single acquisition. This is a representative trace. The oscillations were taking place all along the measurement time of many minutes, not limited to the particular time window sampled by the single acquisition reported here.
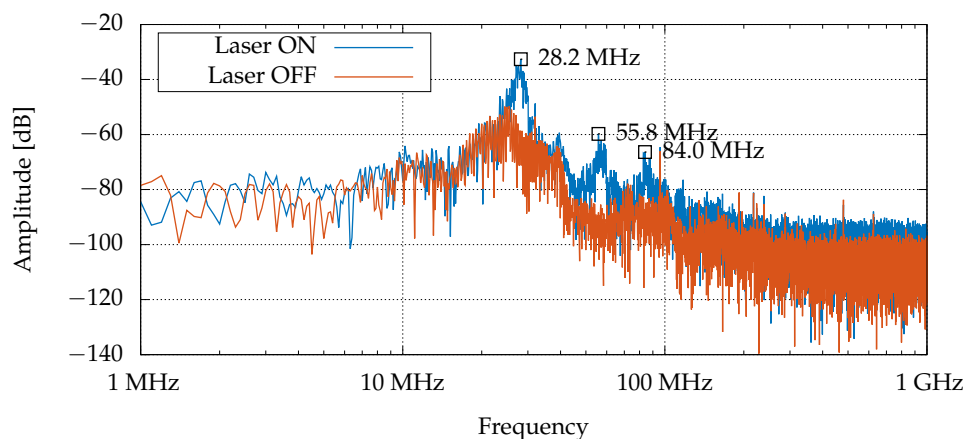
Figure 7. Frequency domain plot of the oscillations for the same case as in Figure 6. The resolution bandwidth of the spectrum analyzer is 100 kHz.
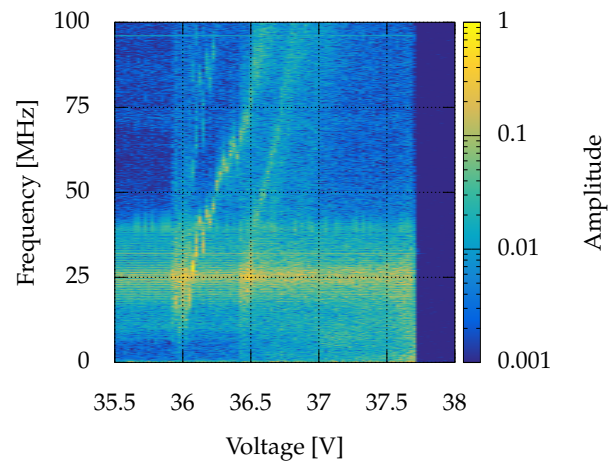
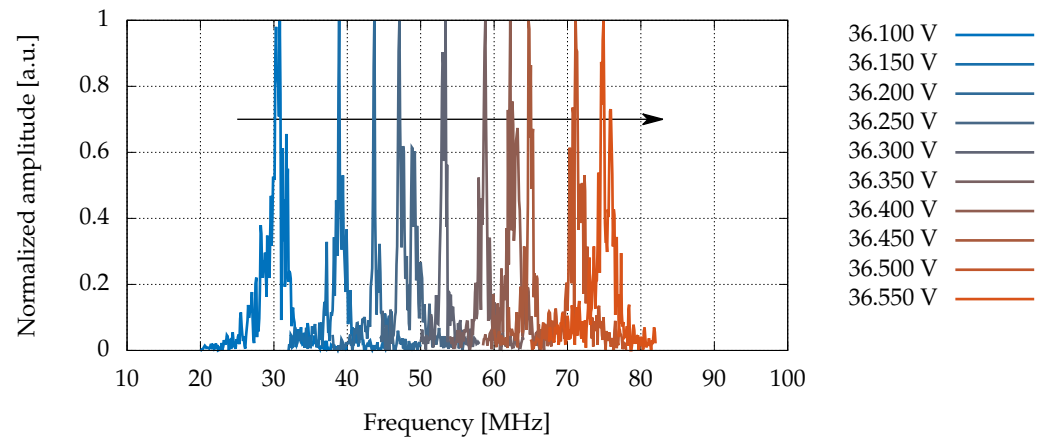**Figure 8.** Normalized spectrogram from 35.5 V to 38 V obtained with TIA 1 which saturates at 37.7 V.

Figure 9. Normalized oscillation peak as the reverse bias voltage increases from 36.100 V to 36.550 V in 50 mV steps.
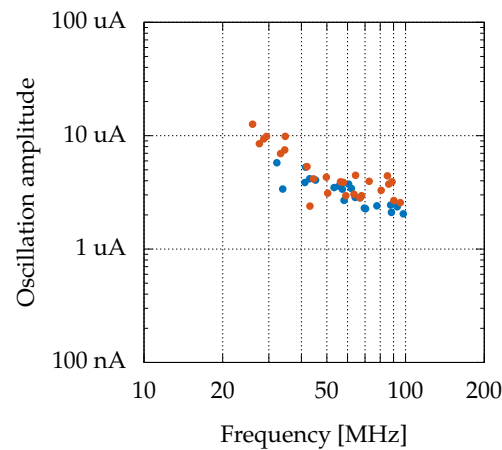

Figure 10. Oscillation amplitude as a function of the frequency of oscillation. The voltage amplitude measured with the oscilloscope has been divided by the transfer function of the TIA to obtain the amplitude in terms of APD current.
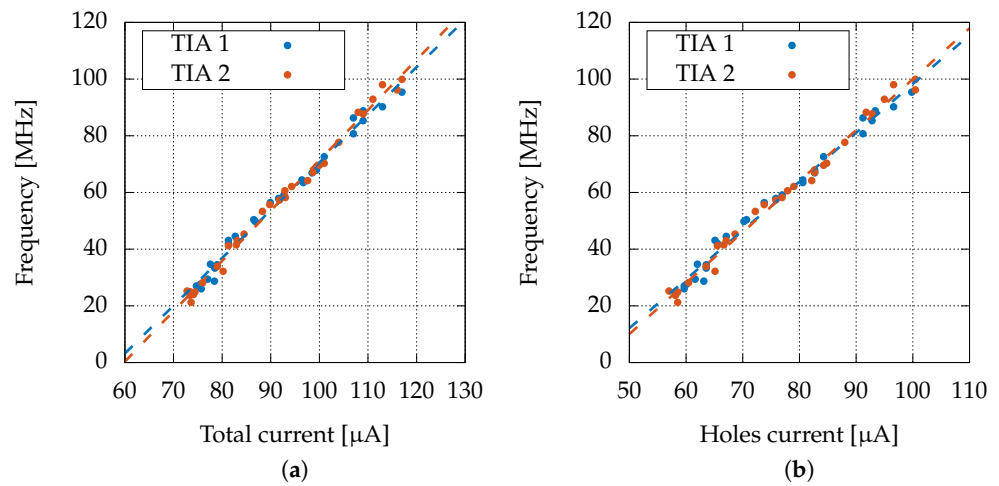
Figure 11. Comparison between measurements performed with different TIAs of the oscillation frequency as a function of (**a**) the total DC current and (**b**) the current associated to holes generated by impact ionization. The laser power is kept constant (P_{laser} = 500 µW) and the current increases since the reverse bias increases.

A closer look to the spectrogram in Figure 8 reveals the presence of multiple harmonics, and all seem to exhibit a linear relationship with the measured current (Figure 12a). Conversely, as expected, the oscillation frequencies do not show a linear dependence with the reverse bias applied (see Figure 12b).

The same measurements (constant laser power and variable reverse bias) were conducted using devices with d_{abs} = 15 µm and 300 nm. For the device with d_{abs} = 15 µm absorption region Figure 13, a similar linear trend of oscillation frequency was observed. However, no oscillations were identified for devices with d_{abs} = 300 nm. Since the devices differ from each other only in their absorption region thickness, we conclude that this fabrication parameter definitely affects the oscillation behavior.
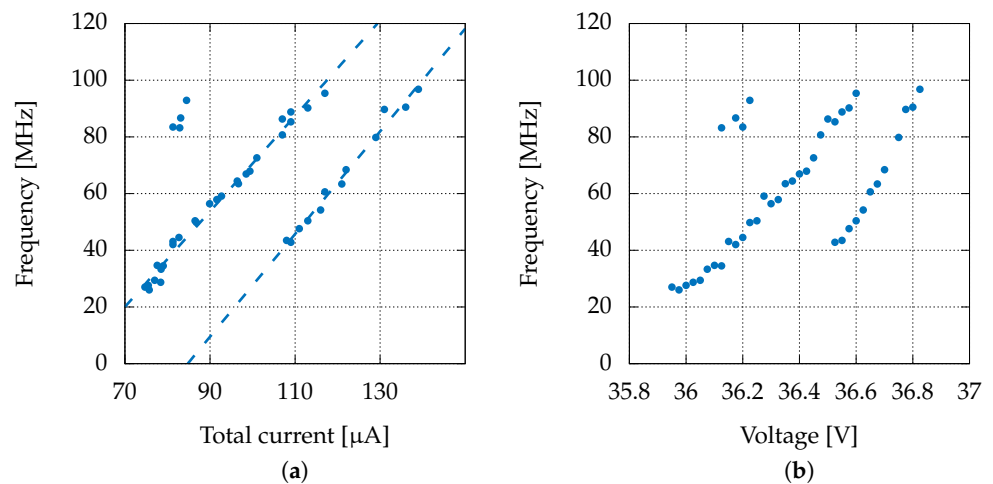

Figure 12. Oscillation frequency as a function of (**a**) DC total current and (**b**) reverse bias.

3.5. Oscillations at Fixed Bias

As previously mentioned, these measurements were carried out increasing the photon flux (laser power from 200 µW to 1 mW) keeping a fixed reverse bias (V = 36.5 V) and therefore a fixed gain value ($M \approx$ 6.5). Figure 14 shows the oscillation phenomenon measured with TIA 1 and $P_{laser} \approx$ 270 µW.

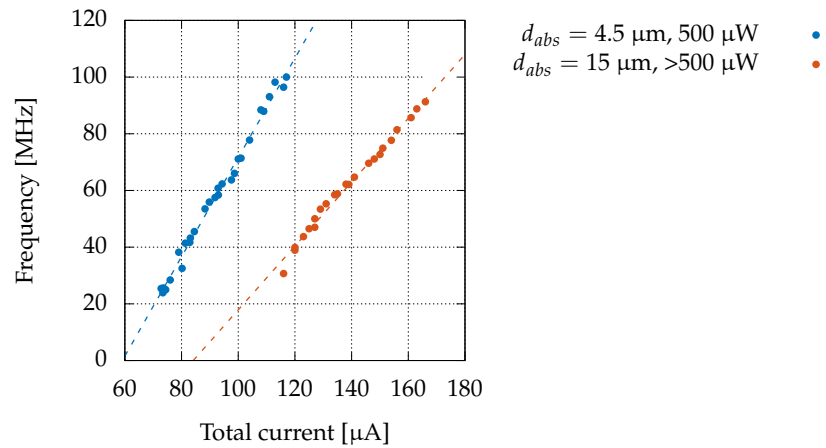**Figure 13.** Oscillation frequency vs. total current: comparison between devices with $d_{abs} = 4.5$ µm and $d_{abs} = 15$ µm. The laser power of the $d_{abs} = 15$ µm was slightly increased above 500 uW to have similar oscillation frequency ranges for the two devices.
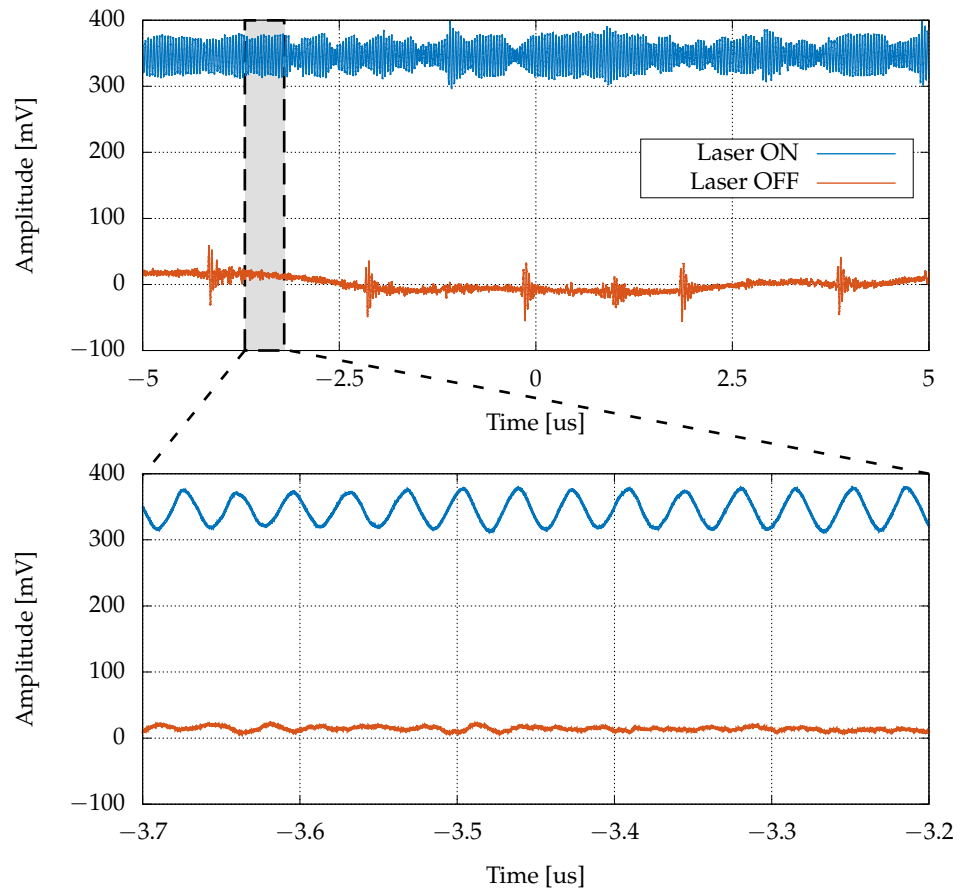

Figure 14. Oscillations in a device with $d_{abs} = 4.5$ µm at fixed bias $V = 36.5$ V measured with TIA 1. Laser power approx. 270 µW.

Even though this characterization differs significantly from the previous one, once more, a clear proportional trend between the oscillation frequency and the measured current (total in Figure 15a, or due to holes generated by impact ionization in the multiplication region Figure 15b) was identified. Also, the slope is rather close in the two cases (fixed laser power or fixed bias), and even closer when measured as a function of the current of holes generated by impact ionization. This suggests that the phenomenon is triggered by

those holes, and that the higher the flux of holes injected back into the absorption region, the faster the process producing the oscillations.
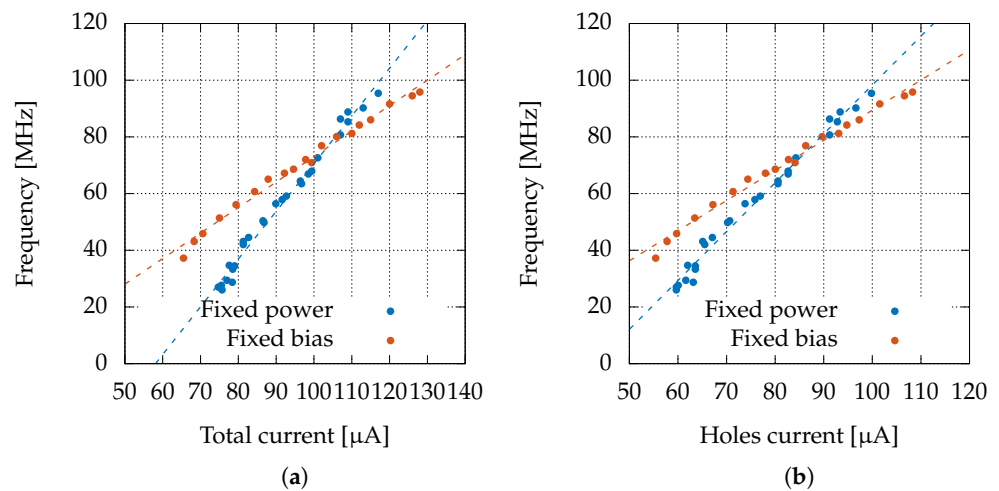

Figure 15. Oscillation frequency trend comparison between measurements with fixed laser power (blue dots, $P_{laser} = 500$ µW) and measurements with fixed bias (red dots, $V = 36.5$ V) as a function of the total DC current (**a**) and the current associated to holes generated by impact ionization (**b**). Device with $d_{abs} = 4.5$ µm.

4. Discussion

We have shown that oscillations in the device's current take place when carrier multiplication by impact ionization becomes significant. If these oscillations were due to a resonance between the APD capacitance and the TIA, possibly also due to inductive effects in the interconnections, the oscillation frequency should change when changing the TIA, but this is not the case, since we found that oscillation frequency and amplitude do not depend on the setup. Furthermore, oscillations associated with the setup are hardly expected to depend on the photon flux and the bias of the APD. For example, the oscillations observed in [13] are due to the interaction between TIA and photodiode: the frequency changes with the TIA parameters (differently to our results) and does not depend on the bias of the photodiode (while it does in our results).

The frequency of these oscillations is essentially linear with the current associated to the holes generated by impact ionization in the multiplication region and injected back into the absorption region. Essentially, the same trend is found with fixed laser power by changing the bias, or at fixed bias by changing the laser power, suggesting that what matters is the current in the device, or, more specifically, the hole current injected back into the absorption region. Of course, at high gains (when the oscillations are visible), the terminal current and the hole current are very close (the former is the photogenerated current multiplied by M, while the latter is the photogenerated current multiplied by $M-1$), and so we obtain similar trends when considering one current or the other. On the other hand, if large currents are induced by the laser before multiplication takes place, no oscillation is observed. This proves that the hole current is the main responsible for the generation of oscillations.

We also see that the thickness of the absorption region plays a key role: devices with thicker absorption regions show a lower frequency of oscillation.

Based on these considerations, we propose a possible interpretation of the oscillating behavior: the photogenerated electrons travel into the absorption region and then, once entering the multiplication region, they generate holes by impact ionization; these holes travel back into the absorption region affecting electron transport therein, leading to a lowering of the electron current itself, so that the number of generated holes decreases too, restoring the initial situation, that again leads to hole injection and so on, so that more electrons get available, increasing again the hole current, and so on. In this view, a larger

hole current will be faster in affecting the absorption region. At the same time, a thick absorption region will require a longer time to be affected by the holes.

To analyze the possible interactions between photogenerated electrons moving forward into the absorption region and impact ionization generated holes moving backward, we performed simulation using a Sentaurus Device [15], where the impact ionization coefficients have been adjusted to roughly reproduce the experimental gain. We first performed DC simulation with constant optical generation, activating or not impact ionization. As can be seen in Figure 16a, the generated holes lower the potential barrier at the junction between the absorption region and the p-layer and induce a small electric field in the absorption region. This lowers the electron concentration in the absorption region, as can be seen in Figure 16b. This large change in the electron charge in the absorption region may trigger a counter effect on the hole concentration and lead to a positive feedback.
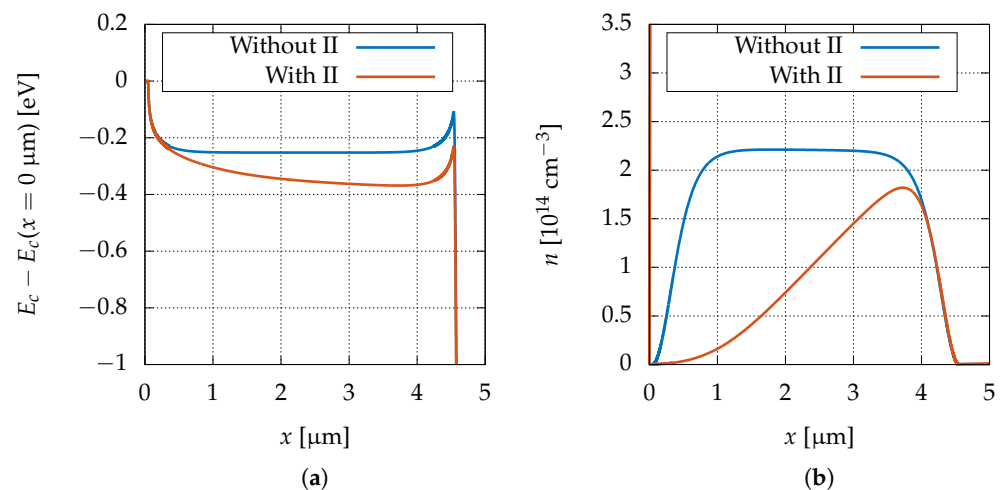

Figure 16. (**a**) Simulated band diagram under optical generation (3.5×10^{18} cm^{-2}s^{-1}) activating or not activating impact ionization, resulting in a gain of approximately 5. (**b**) Corresponding electron concentration profile in the absorption region.

To check if this can produce an oscillating behavior, we resort to transient simulations. The photon flux was approximated by a step function, mimicking a continuous laser flux activated at a given time. Results are reported in Figure 17. We see that without impact ionization, the terminal current smoothly goes from approximately zero to the DC value. On the other hand, when activating impact ionization, we see some oscillation taking place. The period of these oscillations is consistent with the experimental results reported here, and in agreement with experimental findings, it lowers when increasing the optical generation rate. These oscillations are, however, damped. This may be a limitation of the treatment of impact ionization in the TCAD. In fact, the process of carrier generation is not continuous in time, but has a sort of Poissonian nature. So, multiplication taking place at random instants may all the time trigger oscillations such as the ones in Figure 17, making the system present bursts of oscillations.

At the time of this writing, a deepening of this qualitative description is ongoing. The partial success of the simulations based on a Sentaurus Device is a hint that modeling in terms of the simple reaction–diffusion model is not sufficient and must be replaced by an analysis in terms of activator–inhibitor kinetics, which appears to be the suitable mathematical framework needed to describe temporal (as well as spatiotemporal) patterns that may occur in nonlinear dissipative dynamic systems such as semiconductors, as well as surface reactions or autocatalytic chemical reaction systems [16].
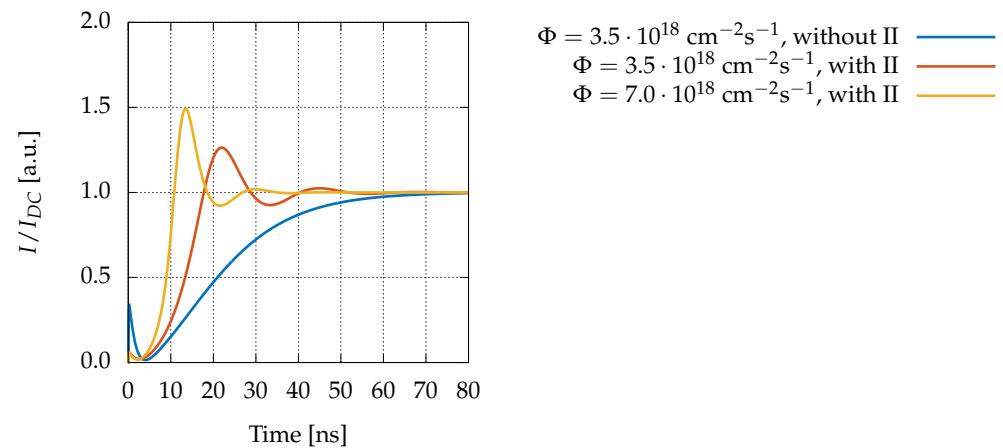
Figure 17. Results of transient TCAD simulations using Sentaurus Device [15]. The photon flux is approximated by a step function. The current is normalized to its DC value. When impact ionization is off, we have a smooth transition toward the steady state DC value, while when II is active, we see damped oscillation.

Author Contributions: Conceptualization, R.H.M., P.P. and G.C.; methodology, P.P. and G.C.; software, M.C. (Matija Colja), M.C. (Marco Cautero) and A.P.; formal analysis, M.B., S.M., P.P., A.P. and G.C.; investigation, M.C. (Matija Colja) and M.C. (Marco Cautero); data curation, M.C. (Matija Colja); writing—original draft preparation, M.C. (Matija Colja), P.P. and G.C.; writing—review and editing, M.C. (Marco Cautero), F.A., M.B., G.B., S.D.Z., F.D., R.H.M., S.M. and A.P.; visualization, M.C. (Matija Colja); supervision, F.D., P.P. and G.C.; project administration, P.P. and G.C.; funding acquisition, G.B., S.D.Z. and G.C. All authors have read and agreed to the published version of the manuscript.

Institutional Review Board Statement: Not applicable.

Informed Consent Statement: Not applicable.

Data Availability Statement: The data presented in this study are available on request from the corresponding author.

Conflicts of Interest: The authors declare no conflict of interest.

Abbreviations

The following abbreviations are used in this manuscript:

APD	Avalanche Photodiode
GaAs	Gallium Arsenide
ENF	Excess Noise Factor
II	Impact Ionization
SAM	Separate Absorption and Multiplication region
PSD	Power Spectral Density
TIA	Transimpedance Amplifier

References

1. Taguchi, K.; Iwanczyk, J.S. Vision 20/20: Single Photon Counting X-Ray Detectors in Medical Imaging. *Med. Phys.* **2013**, *40*, 100901. [CrossRef] [PubMed]
2. Jaszczak, R.J.; Coleman, R.E.; Lim, C.B. SPECT: Single Photon Emission Computed Tomography. *IEEE Trans. Nucl. Sci.* **1980**, *27*, 1137–1153. [CrossRef]
3. Yun, I. *Photodiodes: From Fundamentals to Applications*; InTech: Rijeka, Croatia, 2012.

4. MacLeod, S.J.; See, A.M.; Keane, Z.K.; Scriven, P.; Micolich, A.P.; Aagesen, M.; Lindelof, P.E.; Hamilton, A.R. Radio-Frequency Reflectometry on an Undoped AlGaAs/GaAs Single Electron Transistor. *Appl. Phys. Lett.* **2014**, *104*, 012114,

5. Teich, M.; Matsuo, K.; Saleh, B. Excess Noise Factors for Conventional and Superlattice Avalanche Photodiodes and Photomultiplier Tubes. *IEEE J. Quantum Electron.* **1986**, *22*, 1184–1193. [CrossRef]

6. Nichetti, C.; Steinhartova, T.; Antonelli, M.; Biasiol, G.; Cautero, G.; Angelis, D.D.; Pilotto, A.; Driussi, F.; Palestri, P.; Selmi, L.; et al. Effects of p Doping on GaAs/AlGaAs SAM-APDs for X-rays Detection. *J. Instrum.* **2020**, *15*, C02013. [CrossRef]

7. Williams, G.M.; Compton, M.; Ramirez, D.A.; Hayat, M.M.; Huntington, A.S. Multi-Gain-Stage InGaAs Avalanche Photodiode With Enhanced Gain and Reduced Excess Noise. *IEEE J. Electron Devices Soc.* **2013**, *1*, 54–65. [CrossRef]

8. Pilotto, A.; Nichetti, C.; Palestri, P.; Selmi, L.; Antonelli, M.; Arfelli, F.; Biasiol, G.; Cautero, G.; Driussi, F.; Esseni, D.; et al. Optimization of GaAs/AlGaAs Staircase Avalanche Photodiodes Accounting for Both Electron and Hole Impact Ionization. *Solid-State Electron.* **2020**, *168*, 107728. [CrossRef]

9. Maeda, M.; Minai, Y.; Tanaka, M. Photoinduced Anomalous Oscillations in Reach-through Avalanche Photodiodes. *J. Appl. Phys.* **2008**, *48*, 5324–5327. [CrossRef]

10. Colja, M.; Cautero, M.; Menk, R.H.; Palestri, P.; Gianoncelli, A.; Antonelli, M.; Biasiol, G.; Dal Zilio, S.; Steinhartova, T.; Nichetti, C.; et al. Synchrotron Radiation Study of Gain, Noise, and Collection Efficiency of GaAs SAM-APDs with Staircase Structure. *Sensors* **2022**, *22*, 4598. [CrossRef] [PubMed]

11. Steinhartova, T.; Nichetti, C.; Antonelli, M.; Cautero, G.; Menk, R.H.; Pilotto, A.; Driussi, F.; Palestri, P.; Selmi, L.; Koshmak, K.; et al. Influence of δ P-Doping on the Behaviour of GaAs/AlGaAs SAM-APDs for Synchrotron Radiation. *J. Instrum.* **2017**, *12*, C11017. [CrossRef]

12. Alibava Systems Instruments for Detection. Picoammeter AH501B. Available online: https://alibavasystems.com/producto/picoammeter/ (accessed on 20 June 2023).

13. Wulles, C.; Rafhay, Q.; Desrues, T.; Kaminski, A.; Theodorou, C. Parasitic Oscillation in the Low-Frequency Noise Characterization of Solar Cells. *Solid-State Electron.* **2022**, *194*, 108327. [CrossRef]

14. McIntyre, R. Multiplication Noise in Uniform Avalanche Diodes. *IEEE Trans. Electron Devices* **1966**, *ED-13*, 164–168. [CrossRef]

15. Synopsys Inc. *Sentaurus™ Device User Guide (Version L-2016.03)*; Technical report; Synopsys Inc.: Mountain View, CA, USA, 2013.

16. Schöll, E. *Nonlinear Spatio-Temporal Dynamics and Chaos in Semiconductors*; Cambridge University Press: Cambridge, UK, 2001.